

IMPACT OF TEMPORAL-SPATIO RESOLUTION ON SEA-ICE DRIFT AND DEFORMATION

Cathleen A. Geiger
Center for Climatic Research
Department of Geography
University of Delaware
Newark, Delaware 19716
cgeiger@udel.edu

Mark R. Drinkwater
Oceans/Sea-Ice Unit
European Space Agency
ESTEC Earth Sciences Division
Noordwijk, The Netherlands

Abstract Crafting a zero-mean Gaussian noise numerical experiment, we examine the relationship between the temporal-spatio resolution of any given instrument and the impact that resolution window has on the propagation of error associated with the computation of sea-ice position, velocity, and deformation. These results are characterized through a fitted curve model describing agreement between two data sets (a pure signal and a noise corrupted signal) as a function of time sampling and spatial uncertainty. Using two example instruments (SAR and SSM/I), we demonstrate how this method can be applied to a variety of instruments to estimate the precision of motion vector products given an instrument's chosen temporal and spatial resolution. Relevance to future satellite designs and preprocessing of current data sets is also discussed.

1. Introduction

The displacement of a single sea-ice feature over a period of time describes the drift or velocity of that feature. Mathematically, this is expressed in indicial form as $v_i = \Delta x_i / \Delta t$ for $i = 1, 2, \dots, M$ dimensions, where x_i are components of position, Δx_i the corresponding displacements, and Δt is a chosen time interval. To describe the local drift of a region, velocities from individual features are statistically combined at a suitable spatial scale. Deviations of individual velocities from regional drift indicate spatial variability or local deformation of the field using terms like $\partial v_i / \partial x_j$ for $i, j = 1, 2, \dots, M$ dimensions. These values are computed from chosen spatial scales and at time scales propagated from the individual velocities. Hence, any local field description of drift or deformation depends on both temporal and spatial scales.

In the literature, works by Hibler et al. [1974], Thorndike [1986], Massom [1992], Geiger et al. [1998], Moritz et al. [1999], Padman and Kottmeier [2000], and others have estimated a variety of drift and deformation values using *in situ* buoy trajectories in both Arctic and Antarctic regions. Due to instrumental limitations on the order of 100 to 500 m and specific geophysical interests, most of these studies are designed to resolve features with time scales of a half-day or longer and spatial scales at least the size of the buoy array.

With the recent development of cross-correlation techniques [Fily and Rothrock, 1987; Kwok et al., 1998; Maslanik et al., 1998; Li et al., 1998] and a 2D wavelet method by Liu et al. [1998], sea-ice velocity and deformation are computed from data acquired by remote sensing platforms equipped with microwave radiometers (e.g. SSM/I), Synthetic Aperture Radar (e.g. SAR on ERS-1 and RADARSAT), scatterometers (e.g. Seawinds on QuickSCAT), and others. The texture of these images is resolved into features which can be anything from individual floes to clustered aggregates whose size depends on the resolution of the specific remote sensing platform.

C. A. GEIGER AND M. R. DRINKWATER

Maslanik et al. [1998] compare a number of different tracking methods and show a wide range of agreement between SSM/I-derived motion vectors and buoy drift. In that report, a lower limit RMSE (root mean square error) of 2.8 cm s^{-1} was found between SSM/I and buoy velocity using a 2D wavelet method and a 4-day sliding window [Liu et al., 1998]. Errors increased considerably when time steps were reduced with some of the largest errors seen from 1-day displacements in dynamically active regions (e.g. standard deviation for velocity of 6.9 cm s^{-1} in the Weddell Sea [Kwok et al., 1998]). In each of these studies satellite-derived motion vectors at 100 km and 200 km grid spacing were compared to point source (buoy) motion vectors.

A study by Geiger et al. [2000] improved on these results through the determination of local drift and deformation. Using a collection of sparse gridded motion vectors (from both buoys and satellite products) a spatial scale commensurate with the local dominant forcing was found using a vector RMSE minimization of spatial variability terms ($\partial v_i / \partial x_j$) between buoy and satellite-derived results. As an example, a 600 km 8-buoy array in the Eurasian basin was compared with SSM/I motion vectors at 100 km grid spacing yielding an RMSE of 1.83 cm s^{-1} , 31.0° , $2.47 \times 10^{-8} \text{ s}^{-1}$, and $4.56 \times 10^{-8} \text{ s}^{-1}$ for speed, direction, divergence and shear, respectively. These results were found using a 4-day sliding window and 1000 km spatial scale which matched the temporal and spatial scales of atmospheric storms, respectively.

There are three fundamental difficulties in comparing all of the above methods and results. First, the studies span a considerable range of time scales (anywhere from daily to 7-day sliding or averaging windows). Second, the resolution of the spatial properties of geophysical features is dependent on the chosen temporal scale (e.g. one cannot resolve the spatial variations caused by a 5-day storm with a 7-day time interval even when very high 10 m spatial resolution images are available). Third, while the use of RMSE and standard deviation is meaningful in comparing results at one particular scale, their values vary depending on the magnitude of the property examined. This is particularly true when comparing deformation results which have a much greater range of magnitude than velocity, are highly dependent on local dynamics (tides, storms, strong local ocean currents), and therefore are more sensitive to temporal-spatio scales than velocity.

In this paper, we address some of these temporal-spatio scaling issues via a numerical experiment using random Gaussian noise to demonstrate the propagation of errors. We quantify our ability to compare two data sets as a function of time interval and spatial uncertainty, then discuss and summarize these findings.

2. Methodology

A differential method for computing local sea-ice drift and deformation through statistical means using multiple linear regression is well described in the literature [Hibler et al., 1974; Geiger et al., 1998; Geiger et al., 2000]. We review this method here and further identify the statistics used in evaluating the data sets chosen for this study. While other methods exist which may be more accurate (e.g. integral methods), we have found from earlier works [Hibler et al., 1974; Geiger et al., 2000] that the errors associated with instrumental position uncertainty for sea ice are many times greater than those associated with numerical round-off and truncation errors. Therefore, we make use of the statistical strength of this method to unravel an important data sampling issue.

2.1 LOCAL DRIFT AND DEFORMATION

In-situ buoy arrays are typically sparse in number but capable of providing reasonable deterministic results of local drift and deformation when computed in groups of three and can pro-

TEMPORAL AND SPATIAL RESOLUTION

vide statistically reasonable estimates when clustered in groups of 6 or more [Thorndike, 1986; Geiger et al., 2000]. Using multiple linear regression [e.g. Geiger et al., 1998; Hines and Montgomery, 1990], we solve for the unknowns of local velocity $(v_i)_0$ and associated local derivatives $(\frac{\partial v_i}{\partial x_j})_0$ given known particle velocities $(v_i)_n$ and their distance from a chosen local point $\Delta(x_i)_n = (x_i)_n - (x_i)_0$ based on the Taylor expansion of velocity about a local point of interest $(x_i)_0$ such that

$$(v_i)_n = (v_i)_0 + \left(\frac{\partial v_i}{\partial x_j}\right)_0 (\Delta x_j)_n + \frac{1}{2} \left(\frac{\partial^2 v_i}{\partial x_j \partial x_k}\right)_0 (\Delta x_j \Delta x_k)_n + \dots \quad (0.1)$$

where repeated indices sum; $i, j, k = 1, 2, \dots$ dimensions; $n = 1, 2, \dots$ is indexing known particles; and the index 0 identifies the local point of interest from which $(x_i)_n$ are measured. Speed, direction, and strain-rate invariants of divergence and maximum shear follow from this solution [Geiger et al., 2000].

2.2 STATISTICS

There are a number of statistics that can be applied to a multiple linear regression solution to Eq. (0.1) as shown in Geiger et al. [1998, 2000]. In this study, we focus on two of these. First, we choose the RMSE between two data sets as it is the standard often seen in satellite-derived motion product comparisons, providing a means of comparing results from different studies. For clarity, we define RMSE as

$$RMSE = \sqrt{\frac{1}{K} \sum_k \sum_n \left(S_{nk}^{(1)} - S_{nk}^{(2)}\right)^2} \quad (0.2)$$

where $n = 1$ for the RMSE between scalar quantities of two data sets ($S(1)$ and $S(2)$) indexed in time by k of length K and $n > 1$ to index between multiple components of two data sets (velocity vector $n = 1, 2$; first order derivatives $n = 1, 2, 3, 4$ [Geiger et al., 2000]).

One difficulty with RMSE is that it is derived from the square of the difference of two values, and hence large differences (outliers) have greater weight in the result. A similar amplification of outliers occurs in correlation calculations where there is the added loss of mean information, leaving room for unaccounted errors. Therefore, the second statistical measure we choose is the index of agreement (d) [Willmott et al., 1985] which was developed as a practical alternative to correlation because it scales with the magnitude of the variables, retains mean information, and does not amplify outliers. The formulation for the index of agreement is

$$d_\gamma = 1 - \left[\frac{\sum_{k=1}^K \omega_k |\vec{d}_k|^\gamma}{\sum_{k=1}^K \omega_k (|\vec{p}_k - \bar{\vec{o}}| + |\vec{o}_k - \bar{\vec{o}}|)^\gamma} \right] \quad (0.3)$$

where K is the number of data points observed (\vec{o}_k) and predicted (\vec{p}_k) for either scalar or vector quantities, $\vec{d}_k = \vec{p}_k - \vec{o}_k$ is the difference between predicted and observed, $\bar{\vec{o}} = \sum_{k=1}^K \omega_k \vec{o}_k / \sum_{k=1}^K \omega_k$ is the mean of the observed, ω_k are weight functions, and γ is the order of the index (1=linear, 2=quadratic, etc). According to Willmott (personal communication), the linear form ($\gamma = 1$) is the most robust for comparing results because of its linear approach to a perfect match. In this study, all the data are the same type and there is no redundancy information to gather repeat statistics. We therefore assume the data to be equally weighted and assign $\omega_k = 1$.

3. Experimental Design

We consider two buoy arrays, one is the 6-buoy array from the Ice Station Weddell (ISW) experiment in 1992 from day 65 to 150 located in the perennial ice pack of the western Weddell Sea at the beginning of Austral autumn when the sea ice is expanding [Drinkwater, 1998a]. The array is located at the shelf break in a strong tidal area [Geiger et al., 1998; Padman and Kottmeier, 2000; Foldvik et al., 1990]. Secondly, we consider the 6-buoy array from the Winter Weddell Gyre Study in 1992 (WWGS) [Lemke, 1994; Drinkwater, 1998b] which is located in the seasonal ice zone of the deep basin of the eastern Weddell Sea from day 193 to 335 during Austral Winter through Spring when the sea ice begins to retreat. These two arrays are chosen because they encompass many of the seasonal and regional variations of the Weddell Sea (Figure 1).

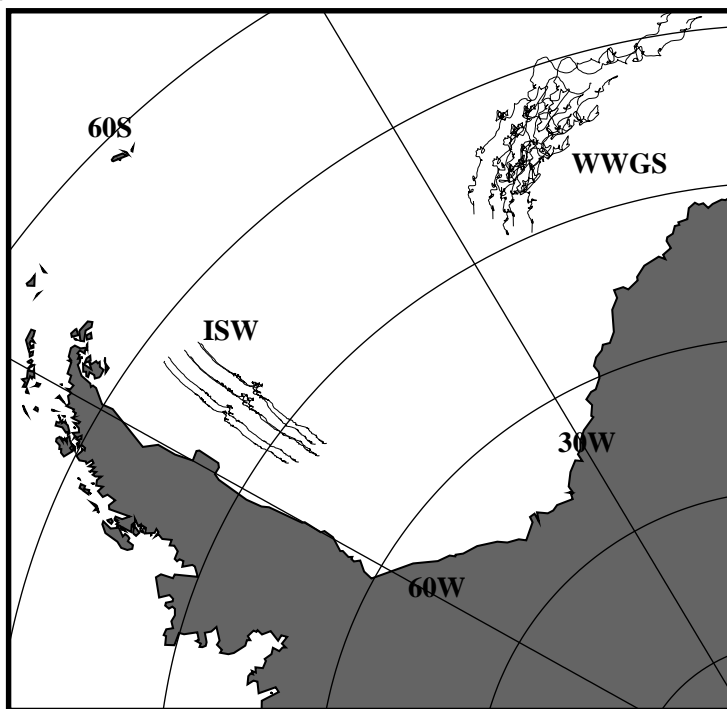


Figure 1. The Weddell Sea region is shown on the SSM/I grid projection. For reference 30°W and 60°W longitude and latitude at 5° intervals are shown. Buoy trajectories from ISW and WWGS experiments from 1992 are superimposed.

For each buoy, we take the hourly linearly interpolated positions (latitude, longitude) and project them onto a polar stereographic SSM/I grid whose y axis is parallel to the 0° meridian. We smooth the position signal using a 9 hour Butterworth 4-pole low-pass filter to minimize the influence of instrument noise [Geiger et al., 1998] while still retaining, for example, most of the strong tidal signal in the ISW buoys. Next we compute velocity using a sliding time window such that $v(t) = (x(t + \Delta t/2) - x(t - \Delta t/2))/\Delta t$ for each hourly reading in each of the 6 buoys in both arrays. For this experiment we choose 6 different time intervals $\Delta t = [1/24, 12/24, 1, 2, 4, 10]$ days, such that we create 6 different velocity time series from the same buoy, each of which has an incrementally smaller amount of high frequency temporal variability (i.e. box car or sliding window filter). We further compute the local drift and deformation

TEMPORAL AND SPATIAL RESOLUTION

at each time relative to the centroid of each array using the multiple linear regression method referenced earlier. We call all of these results original signals.

From earlier findings [e.g. Geiger et al., 2000], we know that the primary source of spatial noise is position error of GPS and ARGOS buoys and temporal-spatio resolution and temporal revisit limitations of remote sensing instruments in the polar regions. To simulate these uncertainties, we make a copy of the original signals' x, y positions. Next, we add random zero-mean Gaussian noise to the copies of x, y positions. To ensure as close to true randomness as possible, we first generate a random seed which is then used to generate the random Gaussian using a standard software random number generator. We multiply each random value by a constant to attain whatever noise level we wish to introduce. In this experiment, we create 46 different noisy signals for each buoy ranging from 10 m to 1000 km including 9 intervals at each base 10 such that we have noise levels [km] of [0.01,0.02,0.03,...,0.1,0.2,0.3,...,1.0,2.0,3.0,...,1000.0]. In other words, each buoy in case 1 has a random Gaussian noise level of 10 m added, case 2 of 20 m, ... case 46 of 1000 km. The range of noise is chosen to reflect the range of resolutions from SAR (10-100 m), GPS/ARGOS (10-500 m), and SSM/I (12.5 km for 85 GHz and 25 km for 37 GHz).

We compute velocity from the noisy x, y positions using the same sliding window method described earlier at the six Δt displacement window ranges and further compute local drift and deformation of the two arrays. In this way, we propagate position uncertainty through both the temporal computation of velocity and the temporal-spatio computation of deformation (e.g. $\Delta u/\Delta x$). Including the original signal which has no noise relative to itself, we generate a total of 47 different spatial noise levels relative to an original signal at 6 different time sampling intervals using 2 buoy arrays from distinct regions of the Weddell Sea. We use these results to examine the relationship between temporal and spatial resolution in the determination of sea-ice drift and deformation.

4. Experimental Results

Three sets of scatter plots are used to highlight the results found. The first is the example shown in Figure 2 (a-d), constructed from the WWGS buoy array from day 193 to 335 using a one day sliding time window and spatial noise of 50 m. Using the index of agreement d as a guide, we notice that speed (Figure 2a) and direction (Figure 2b) show nearly perfect agreement (99.8% and 99.9%, respectively) with very good agreement for divergence and shear (97.9% and 98.6%, respectively).

Next we see in Figure 2(e-h) what happens as we increase the spatial noise (spatial uncertainty equivalent) from 50 m to 900 m. Notice, while the velocity results degrade only slightly (down to 96.6% and 98.3%, respectively), divergence and shear now only moderately agree (67.4% and 76.3%, respectively). By experimental design, the degradation of agreement from velocity to strain-rate invariants can only be attributed to the propagation of error which is amplified as it proceeds from position (noise introduction), to velocity computation, to first-order derivatives of velocity (deformation).

The third example shown in Figure 2(i-l), illustrates what happens when the noise is increased from 900 m to 3 km. While we again see a small reduction in velocity agreement (down from 96.6% to 88.8% for speed and from 98.3% to 94.7% for direction) there is a big change in both the scatter pattern and agreement of the strain-rate invariants (down from 67.4% to 35.0% for divergence and from 76.3% to 39.4% for shear). This third example elucidates how much more sensitive deformation properties are to increasing instrumental uncertainties.

To summarize these results more comprehensively, we construct plots of agreement (d) from all 47 noise levels at each time interval (Figure 3) with ISW results are shown in top panels and WWGS in bottom panels. Grey vertical bars are used to approximate the noise equivalent of

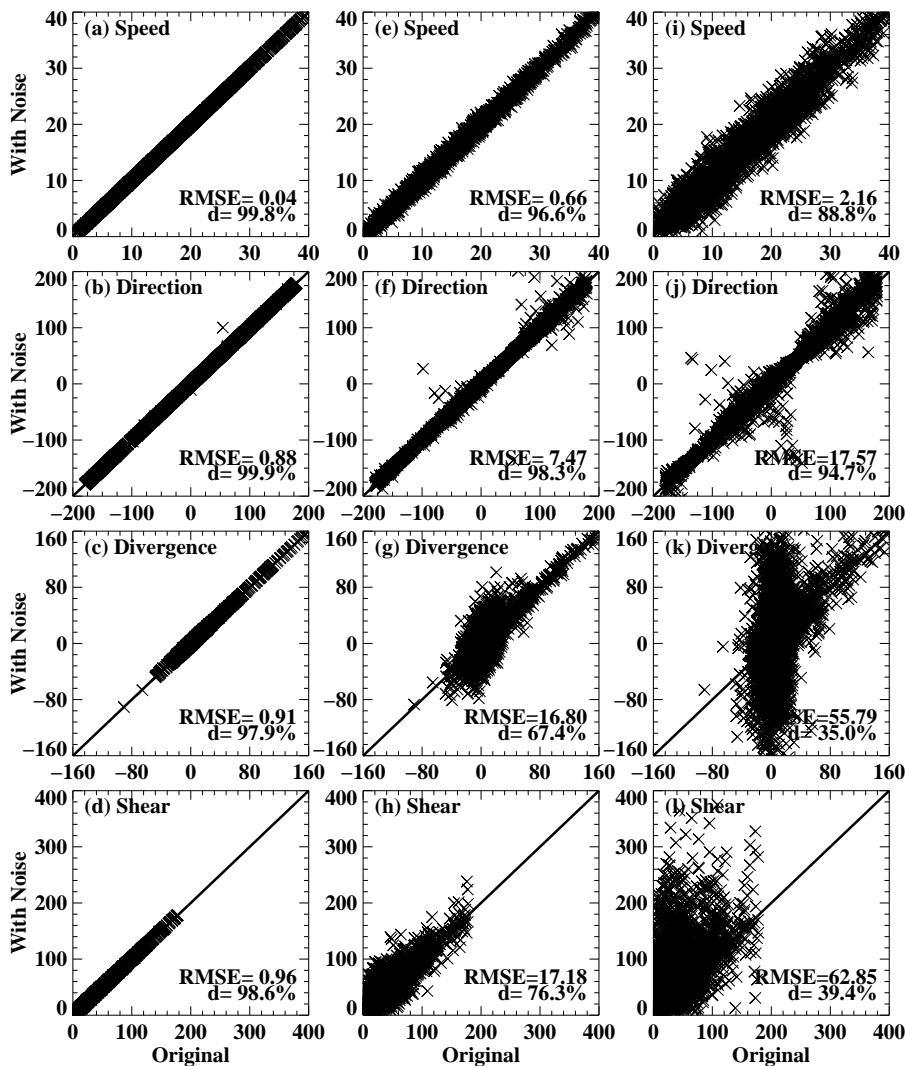


Figure 2. Example results using the WWGS buoy array and a one day time displacement to compute velocity. The abscissa values are properties of speed (cm s^{-1}), direction (degrees), divergence ($\times 10^8 \text{ s}^{-1}$), and shear ($\times 10^8 \text{ s}^{-1}$) derived from the original signal. The ordinate values are computed from the original x, y positions perturbed with zero-mean Gaussian noise levels of 50 m (a-d), 900 m (e-h), and 3000 m (i-l).

SAR-derived and SSM/I-derived motion product resolution (as rough estimates 100 m and 20 km chosen, respectively). Using the grey bars as examples, we see that an instrument with a spatial resolution of the order of ERS-1 SAR (leftmost bars) should agree well against a perfect result ($> 99\%$ for velocity and $> 80\%$ for divergence and shear with very low error propagation for all but the shortest time intervals ($\Delta t < 1$ day).

For SSM/I (rightmost bars), the potential for error propagation is much greater due to the increased spatial uncertainty which infiltrates position estimates as noise thereby increasing the amount of error propagated to velocity and associated derivatives. This is seen in Figure 3 by the shift to the left of divergence and shear agreement relative to speed agreement. In the study by

TEMPORAL AND SPATIAL RESOLUTION

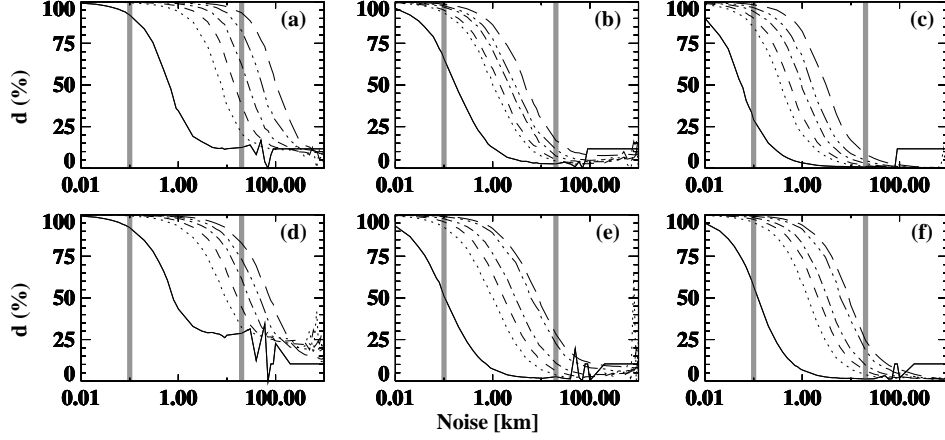


Figure 3. The linear index of agreement (ordinate axis) is plotted for the invariant properties of speed (a,d), divergence (b,e), and maximum shear (c,f) using the buoy arrays from ISW (top panels) and WWGS (bottom panels). The abscissa is the magnitude of the zero-mean Gaussian noise added to the position information. Each curve is characterized by its time displacement, namely one hour (solid), half day (dot), one day (short dash), two days (dot-dash), four days (dot-dot-dot-dash), and ten days (long-dash). The vertical shaded bars denote the approximate resolution (i.e. position uncertainty) of SAR (~ 100 m) and SSM/I (~ 20 km).

Geiger et al. [2000], a dependence on the number of particles was found to significantly impact the signal-to-noise ratio in strain-rate determination, and so we suspect that the two examples shown here using 6 buoys serve as a lower limit estimate with better results possible through the incorporation of more particles.

All the lines in Figure 3 have a similar shape allowing us to mathematically model agreement as a function of time interval and spatial noise. We fit these curves with the function

$$d = \frac{A}{1 + (x/x_0)^p} \quad (0.4)$$

where d is the index of agreement; A is the maximum amplitude (100%); x is the noise level; $p = 2/\ln(s)$; and s is the steepness or slope of the curve near the midpoint x_0 where $d(x_0) = 50\%$. The slope s is estimated as an average using values between $d = 75\%$ and 25% . Averages for slope s (Table 1) are found out of a possible range from 0 (totally vertical) to ∞ (totally horizontal). Visually, we see from Figure 3 that all these curves have similar steepness and their standard deviations are small (Table 1). Hence we estimate an overall average of $s \sim 5$ for this experiment.

Using the individual averages for s shown in Table 1 there remains only one unknown x_0 which we solve for using Eq (0.4) and $d(x_0) = 50\%$. Since agreement drops with increased noise, x_0 can be thought of as the 50% noise tolerance level. While steepness s has a fairly constant value in all cases examined ($s \sim 5$), we note that x_0 (Table 2) increases at a systematic rate for velocity by a factor of ~ 8 between hourly and semi-diurnal time steps, and a doubling in noise thereafter corresponding roughly to each doubling in time intervals (0.5, 1, 2, 4, and 10 days). This result is anticipated since individual velocities are linearly dependent on Δt (i.e. $v_i = \Delta x_i / \Delta t$) and local velocity is based on multiple linear regression, also a linear propagation of time difference.

Table 1 Slopes (s) of Fitted Curves using Eq. (0.4)

	ISW			WWGS		
	VM	DV	MS	VM	DV	MS
mean	3.77	5.69	4.07	5.14	6.90	4.41
s.d.	0.23	0.26	0.39	0.05	1.03	0.41

VM, DV, and MS are abbreviations for the invariants of velocity magnitude (i.e. speed), divergence and maximum shear, respectively. Standard deviation is denoted by the abbreviation s.d.

Table 2 Noise Levels (x_0 [km]) of 50% Agreement from Eq. (0.4)

Δt (days)	ISW			WWGS		
	VM	DV	MS	VM	DV	MS
1/24	0.65	0.17	0.05	0.82	0.14	0.15
12/24	7.04	1.04	0.36	8.68	1.79	1.25
1	14.35	1.37	0.55	16.22	1.98	2.44
2	27.60	2.09	0.94	27.80	3.65	3.83
4	51.77	2.81	1.50	45.25	7.31	7.43
10	107.60	4.46	3.00	77.66	8.62	9.23

Figure 3 and Table 2 also show how strain-rate invariants are more sensitive than velocity in two distinct ways. First, as seen in Figure 3, much lower noise levels are necessary to reach tolerable levels of agreement. Comparing 50% noise tolerance x_0 values on the same row in Table 2, we note that strain-rates reach 50% agreement at noise levels which are anywhere from 4 to 40 times as small as velocity. Secondly, comparing x_0 values in the same column, we see how much slower strain-rate invariants reach 50% agreement as time interval is increased. Compared with the linearly varying velocity results, this result suggests a non-linear relationship between temporal-spatio scaling and the quality of deformation results.

Compared to the WWGS buoy array, the index of agreement for the ISW buoy array (Figure 3) shows similar spatial and temporal sampling behavior for velocity with only slightly less agreement as spatial noise is increased (i.e. less steepness, higher s value). A higher tolerance for noise is found in the strain-rate invariants for the WWGS array than the ISW array by roughly a factor of 2. There is no apparent pattern when comparing x_0 results between divergence and shear which could be due to a number of issues. While x_0 clearly depends on the time interval, we suspect it is further dependent on the number of features/particles. The remaining differences may be attributed to the scale and location of the features (e.g. storm systems versus tidal, deep versus shallow water) but this requires a more extensive study than is possible here.

5. Discussion and Summary

Summarizing this experiment, we are able to quantify the propagation of noise through position, local velocity, and deformation properties. We make use of these results to further characterize data set agreement as a function of time interval and spatial noise via a fitted curve model. The steepness (s) of this function relates to how quickly agreement deteriorates with increasing spatial noise, which we find to be $s \sim 5$ for the Weddell Sea when considering both Austral autumn and winter to spring conditions, varying geophysical regions and processes (tides, storms, perennial versus seasonal pack ice, and others). The systematic increase in x_0 with increasing time interval additionally describes the deterioration of agreement with spatial noise but in the form of a constant offset thus providing a mathematical link between temporal and spatial

TEMPORAL AND SPATIAL RESOLUTION

choices of scale at least for velocity. An overlay of spatial uncertainty for SAR and SSM/I instruments via grey bars in Figure 3 further illustrates the impact of error propagation and its dependence on spatial and temporal scales.

Numerical experiments and scaling arguments shown here reveal similar results to Geiger et al. [2000] for the Arctic, namely that error propagation has a serious impact upon the quality of deformation quantities. This is particularly true of satellite-derived deformation statistics. Using the statistical method chosen here, we are able to keep track of these errors and, concurring with Geiger et al. [2000], believe that Antarctic results can be further improved by increasing the number of particles. Since it is spatial variability and associated deformation processes that determine the compactness of sea ice, the propagation of these errors will continue through any application of motion fields to mass balance calculations as they are highly dependent on spatial variability estimates in determining ice growth. Thus errors should be carefully addressed and great care applied to motion vector products in climate applications and process studies, for example.

The relationship found here between index of agreement, time interval, and spatial uncertainty, while a very useful quantitative measure, is probably regionally dependent and case specific such that little generalization can be made at this point about values of s and x_0 in Eq. (0.4) based solely on this study. An extension of this model should include the impact of number of particles and probably the scale of geophysical processes before the formulation is applied in a more general way. In its current form Eq. (0.4) is a simple measure between temporal and spatial scales versus potential data quality given instrument resolution. A useful application of the fitted curve model could be its incorporation into satellite-derived motion product preprocessing as a gauge for selecting appropriate temporal and spatial scales before applying them to models or other studies. It may also serve as a useful tool in devising future polar satellite deployment strategies in an effort to adequately resolve the processes of greatest concern to the community at large.

Acknowledgments

Work performed by CAG at the University of Delaware was supported by funding through NSF Grant OPP9818645. Work performed by MRD was undertaken at Jet Propulsion Laboratory under contract to the National Aeronautics and Space Administration through NASA Code Y research awards 665-21-02 and 621-21-02. Thanks goes to Christoph Kottmeier for the WWGS buoy data and Steve Ackley for the ISW buoy data. CAG also thanks Cort Willmott for many interesting discussions on data comparison techniques. Finally, we thank the anonymous reviewers whose comments led to improvements in the paper.

References

- Drinkwater, M.R., 1998a. Active Microwave Remote Sensing Observations of Weddell Sea Ice. In *Antarctic Sea Ice: Physical Processes, Interactions and Variability*, Anarct. Res. Ser. **74**: 187-212. Ed. M.O. Jeffries, AGU, Washington, D.C.
- Drinkwater, M.R., 1998b. Satellite Microwave Radar Observations of Antarctic Sea Ice. In *Analysis of SAR Data of the Polar Oceans*, **8**: 145-187, Eds. C. Tsatsoulis and R. Kwok, Springer-Verlag, Berlin.
- Fily, M. and Rothrock D.A., 1987. Sea ice tracking by nested correlations. *IEEE Trans. Geosci. Remote Sens.* **25**: 570-580.
- Foldvik, A., Middleton, H.H., and Foster, T.D., 1990. The tides of the southern Weddell Sea. *Deep Sea Res.* **37**: 1345-1362.

C. A. GEIGER AND M. R. DRINKWATER

- Geiger, C.A., Zhao, Y., Liu, A.K., Häkkinen, S.M., 2000. Large-scale comparison between buoy and SSM/I drift and deformation in the Eurasian Basin during winter 1992-1993. *J. Geophys. Res.* **105**: 3357-3368.
- Geiger, C.A., Ackley, S.F., and Hibler III, W.D., 1998. Sea ice drift and deformation processes in the western Weddell Sea. In *Antarctic Sea Ice: Physical Processes, Interactions and Variability*, Anarct. Res. Ser. **74**: 141-160. Ed. M.O. Jeffries, AGU, Washington, D.C.
- Hibler III, W.D., Weeks, W.F., Kovacs, A., and Ackley, S.F., 1974. Differential sea ice drift. Part 1: Spatial and temporal variations in sea ice deformation. *J. Glaciol.* **13**: 437-455.
- Hines, W.W. and Montgomery, D.C., 1990. Multiple Regression. In *Probability and Statistics in Engineering and Management Science*. (3rd Edition) **15**: 487-558. John Wiley, New York.
- Kwok, R., Schweiger, A., Rothrock, D.A., Pang, S., and Kottmeier, C., 1998. Sea ice motion from from satellite passive microwave imagery assessed with ERS SAR and buoy motions. *J. Geophys. Res.* **103**: 8191-8214.
- Li, S., Cheng, Z., and Weeks, W.F., 1998. Extraction of intermediate scale sea ice deformation parameters from SAR ice motion products. In *Analysis of SAR Data of the Polar Oceans*. pp. 69-90 Eds. C. Tsatsoulis and R. Kwok, Springer-Verlag, New York.
- Lemke, P. (editor), 1994. The expedition ANTARKTIS X/4 of R/V Polarstern in 1992. *Reports on Polar Research 140*, pps. 99. Alfred Wegener Institut für Polar- und Meeresforschung, D-27568, Bremerhaven, Germany.
- Liu, A.K. and Cavalieri, D.J., 1998. On sea ice drift from the wavelet analysis of the Defense Meteorological Satellite Program (DMSP) Special Sensor Microwave Imager (SSM/I) data. *Int. J. Remote Sens.* **19**: 1415-1423.
- Massom, R. A., 1992. Observing the advection of sea ice in the Weddell Sea using buoy and satellite passive microwave data. *J. Geophys. Res.* **79**: 15559-15572.
- Maslanik, J., Agnew, T., Drinkwater, M.R., Emery, W., Fowler, C., Kwok, R., and Liu, A.K., 1998. Summary of ice-motion mapping using passive microwave data. pp. 1-25. Boulder, CO: *Report prepared for the Polar Data Advisory Group*, NASA Snow and Ice Distributed Active Archive Center, National Snow and Ice Data Center.
- Moritz, R.E., Runciman, K.A., and Colony, R., August 1999. Observed variability of monthly sea ice velocity and surface geostrophic winds: 1979-1996. *Proceedings from The Arctic Buoy Programme*, Seattle, Washington, USA, 3-4 August, 1998. Sponsored by WMO/IOC, International Arctic Buoy Programme, IAPO Informal Report No. 4.
- Padman, L., and C. Kottmeier, 2000. High-frequency ice motion and divergence in the Weddell Sea. *J. Geophys. Res.* **105**: 3379-3400.
- Thorndike, A.S., 1986. Kinematics of sea ice. In *The Geophysics of Sea Ice*. NATO ASI Series, Series B, Vol. 146. **7**: 489-549. Ed. N. Untersteiner, Plenum, New York.
- Willmott, C.J., Ackleson, S.G., Davis, R.E., Feddema, J.J., Klink, K.M., Legates, D.R., O'Donnell, J., and Rowe, C.M., 1985. Statistics for the evaluation and comparison of models. *J. Geophys. Res.* **90**: 8995-9005.